CONSTITUTIVE BEHAVIOR MODELING AND FRACTIONAL DERIVATIVES

Chr. Friedrich[a], H. Schiessel[b] and A. Blumen[b]

[a]Freiburg Materials' Research Center, Freiburg University, Stefan-Meier-Str. 21, 79104 Freiburg, Germany

[b]Theoretical Polymer Physics, Freiburg University, Rheinstr. 12, 79104 Freiburg, Germany

1. INTRODUCTION

The simplest decay behaviors are exponential, such as the dielectric relaxation associated with Debye and the mechanical relaxation named after Maxwell. Exponential decays depend on a single mode (or, equivalently, a single characteristic time). But most relaxation processes are governed by a large variety of characteristic times, see references [1-4] for reviews, and vast types of decay patterns follow, most popular being stretched exponentials (Kohlrausch-Williams-Watts [2,5,6]) and power law behaviors. In this review we focus on the cases in which the decay function follows a power law for reasonably extended time or frequency intervals. Note that too short time or frequency windows do not allow to distinguish between different decay patterns [7].

The transition from the glassy relaxation zone to the transitional zone in the case of stress relaxation of a glassy polymer is an example for power-law relaxation. Consider polyisobutylene at the reference temperature $T_0 = 25°C$: In Figure 1(a) we reproduce, following reference [8] its shear storage and loss moduli G' and G'' as a function of the frequency ω; in Figure 1(b) we display the corresponding shear relaxation modulus G and the shear creep compliance J as a function of time. As is evident by inspection, the high modulus plateau is followed by a power law that covers about four decades in time (Figure 1(b)) and frequency (Figure 1(a)). Then a second plateau zone (called the entanglement plateau) shows up. This transition from one plateau to another, generally via a power law, is characteristic for amorphous polymers.
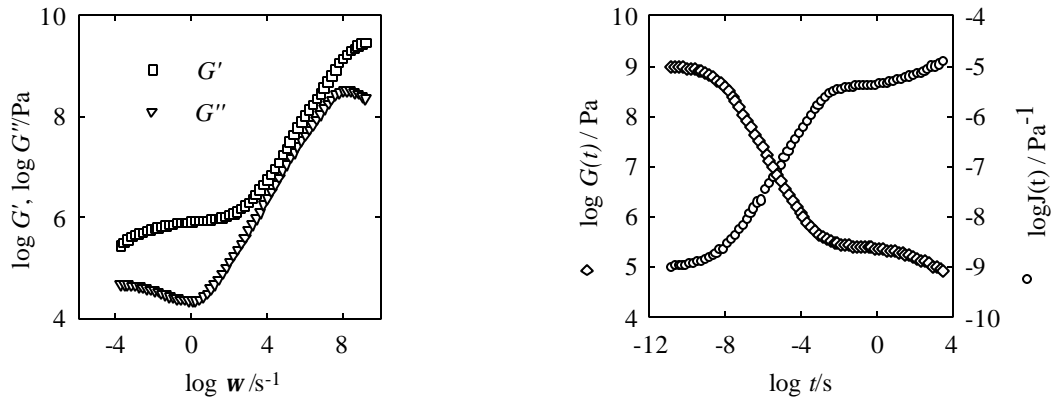
Figure 1(a). Storage modulus $G'(w)$ and loss modulus $G''(w)$ for polyisobutylene as a function of frequency. The data are from Tobolsky and Catsiff [8].

Figure 1(b). Relaxation function $G(t)$ and creep function $J(t)$ for polyisobutylene (as in figure 1(a)) as a function of time.
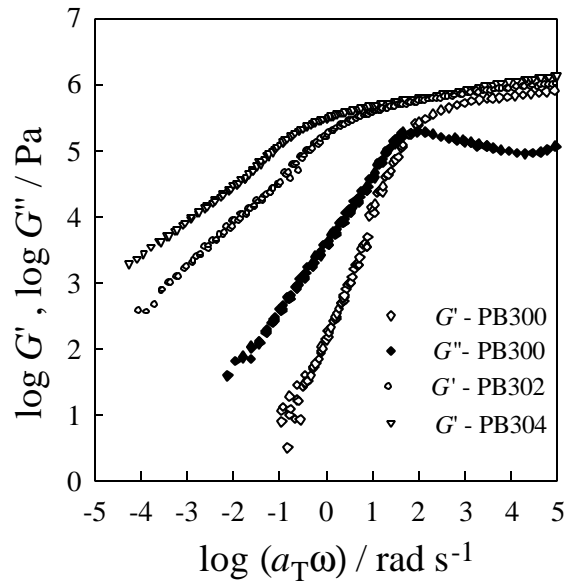

Figure 2. Storage modulus G' and loss modulus G'' of unmodified (PB300) and urazole modified polybutadiene (PB302 and PB304) vs. the reduced frequency $a_T w$. The molecular weight of all samples is $M_W = 31$ kg/mol; the samples 302 and 304 correspond to the 2 mol % and to the 4 mol % modification, respectively.

Furthermore, power law behaviors also appear in the terminal relaxation zone of polymers. In the case of a single relaxation time one has a sharp transition from the entanglement plateau to the flow zone, which obeys a typical liquid-like behavior, namely $G' \propto w^2$ and $G'' \propto w$. Physically or chemically cross-linked polymers [9], polymers with star-, H-, or comb-like topologies (see e.g. [10-19]) show a more general pattern, namely an intermediate power-law domain with $G' \propto w^a$ and $G'' \propto w^b$, where α and β lie between zero and one. In Figure 2 we contrast the behavior of neat, monodisperse polybutadiene to that obtained by attaching to its backbone active groups, which are able to form H-bonds. While for neat polybutadiene the shear storage and loss moduli obey $G' \propto w^2$ and $G'' \propto w$, the moduli of the modified polymers follow more general power laws. The reason for this behavior is that the active groups form temporary, random links between the polymers, fact which renders the relaxation process multimodal and cooperative; this leads here to power laws. Such laws are not the hallmark of polymers only; vast classes of substances, which range from inorganic glasses to proteins show such behaviors [1], and we like to recall the early works of Meinardi et al. [20-22] on power law relaxation in metals, in rocks and in glasses.

In this chapter we focus on the possibility to portray such complex viscoelastic features of polymers by means of fractional calculus, a formalism which turns out to be exceedingly well-suited for this purpose. To this effect we start here by illustrating, using a simple example, how fractional calculus comes into play as a result of the superposition principle. We start with $G(t)$, the *shear relaxation modulus* of a linear system. Now $G(t)$ is defined as the response of the shear stress $t(t)$ to a jump in the shear strain $g(t) = g_0 Q(t)$ where $Q(t)$ is the unit step function. We assume that $G(t)$ obeys a power law, i.e.

$$G(t) = \frac{E}{G(1-b)}\left(\frac{t}{l}\right)^{-b} \tag{1}$$

with $0 \le \beta < 1$. In equation (1) E and λ are constants and $G(x)$ denotes the Gamma function [23]; for convenience we chose in equation (1) the prefactors in such a way as to conform to the main body of the Chapter. Due to the linearity of the system, the response of the stress to a previous history of deformations $g(t)$ is given by the superposition integral [24,25]:

$$t(t) = \int_{-\infty}^{t} dt' \, G(t-t')\frac{dg(t')}{dt'} \quad . \tag{2}$$

Inserting $G(t)$ given by equation (1) into equation (2) we have

$$t(t) = \frac{E\boldsymbol{l}^b}{\boldsymbol{G}(1-\boldsymbol{b})} \int_{-\infty}^{t} dt' (t-t')^{-b} \frac{d\boldsymbol{g}(t')}{dt'} \qquad (3)$$

Now equation (3) can be rewritten in the following compact form

$$t(t) = E\,\boldsymbol{l}^b \frac{d^b \boldsymbol{g}(t)}{dt^b} \;, \qquad (4)$$

in which d^β/dt^β denotes the fractional derivative of order β [26,27] (see section 2 for details). Equation (4) with $0 < \beta < 1$ interpolates between Hooke's law describing solid behavior ($\beta = 0$), i.e.

$$t(t) = E\boldsymbol{g}(t) \qquad (5)$$

and Newton's law describing fluid behavior ($\boldsymbol{b} = 1$)

$$t(t) = \boldsymbol{h}\frac{d\boldsymbol{g}(t)}{dt}. \qquad (6)$$

Equation (4) is an example of a rheological constitutive equation (RCE) with fractional derivatives. As we proceed to show below, a whole series of complex behavior patterns (including crossover situations as discussed above) can be described by relatively simple fractional RCEs.

This Chapter is organized as follows: In the next section we give a brief introduction to fractional calculus. After surveying the historical development of fractional RCEs in section 3, we discuss in section 4 the representation of such RCEs by mechanical analogues. In section 5 we highlight the usefulness of the formalism by applying the fractional Maxwell and Kelvin-Voigt models to a variety of polymeric systems. In section 6 we discuss more complex fractional models. Finally, we conclude with a summary in section 7 and relegate some important but more mathematical expressions to the Appendix.

2. FRACTIONAL DIFFERENTIATION AND INTEGRATION

The straightforward extension of classical calculus to its fractional counterpart is most readily visualized by using a notation which unifies ordinary integration and differentiation:

$$\frac{d^a f(t)}{dt^a} = \begin{cases} f^{(a)}(t) , & \text{for } a = 1,2,3,..., \\ f(t) , & \text{for } a = 0, \\ \int_{-\infty}^{t} dt_1 \int_{-\infty}^{t_1} dt_2 ... \int_{-\infty}^{t_{-a-1}} dt_{-a} f(t_{-a}) , & \text{for } a = -1,-2,-3,... \end{cases} \tag{7}$$

together with the *Weyl integral* [27]:

$$\frac{d^a f(t)}{dt^a} = \frac{1}{G(-a)} \int_{-\infty}^{t} dt' \frac{f(t')}{(t-t')^{a+1}} \tag{8}$$

One has only to realize that for $a = -1,-2,-3,...$ equation (8) is nothing but Cauchy's formula for repeated integration [26,27]; hence for these values of α equations (7) and (8) are equivalent. Now, the basic idea is that equation (8) can be readily extended to all $\alpha < 0$; this defines *fractional integration*. The extrapolation to the positive α–range, $a > 0$, is obtained by first picking an integer n, $n > \alpha$, then performing a fractional integration of order $a - n$, followed by an ordinary differentiation of order n, i.e. [26,27]

$$\frac{d^a f(t)}{dt^a} = \frac{d^n}{dt^n} \left(\frac{d^{a-n} f(t)}{dt^{a-n}} \right) . \tag{9}$$

Equation (9) defines *fractional differentiation*.

Let us note that also another version of fractional calculus, the so-called *Riemann-Liouville (RL) formalism* [26,27], is of widespread use in rheology. In RL the lower limit of the integrals in equations (7) and (8) is set to 0. The RL formalism is particularly suitable for studying the transient response of materials after switching an external perturbation on, say at $t = 0$, so that $t(t) = g(t) \equiv 0$ for $t < 0$. In this spirit the RL version can be understood as being the restriction of the Weyl formalism to a special class of initial value problems. In the following we will use the Weyl formalism; the translation into the RL version is straightforward.

Weyl's fractional calculus turns out to be algebraically very convenient: the composition rule for differentiation and integration obeys the simple form

$$\frac{d^m}{dt^m}\frac{d^n f}{dt^n} = \frac{d^{m+n} f}{dt^{m+n}}$$ (10)

for arbitrary μ and ν [27]. Furthermore, the Fourier transform

$$\mathcal{F}\{f(t)\} = \tilde{f}(w) = \int_{-\infty}^{\infty} dt\, f(t)\exp(-iwt)$$ (11)

turns the operation d^α/dt^α into a simple multiplication [26,27]

$$\mathcal{F}\left\{\frac{d^a f(t)}{dt^a}\right\} = (iw)^a\, \tilde{f}(w)\ .$$ (12)

Let us illustrate the usefulness of these properties using the above-mentioned rheological example. A quick comparision of equation (3) with the Weyl integral, equation (8), leads immediately to the fractional stress-strain relation

$$t(t) = El^b\, \frac{d^{b-1}}{dt^{b-1}}\frac{dg(t)}{dt}\ .$$ (13)

Furthermore using the composition rule, equation (10) with $m = b - 1$ and $n = 1$, equation (13) turns into equation (4), as stated in the previous section.

The behavior of fractional derivatives under Fourier transformation is especially useful in determining the dynamical response functions. Let us consider the *complex shear modulus*

$$G^*(w) = iw\int_0^\infty dz\, G(z)\exp(-iwz)$$ (14)

which describes the response of the stress to a harmonic strain excitation $g(t) = g_0 \exp(iwt)$. From equation (2) it follows by the change of variables $z = t - t'$ that $\tilde{t}(w) = G^*(w)\,\tilde{g}(w)$. Using the multiplication rule, equation (12), one finds, say from equation (4):

$$G^*(w) \equiv \tilde{t}(w) / \tilde{g}(w) = E(iwl)^b . \tag{15}$$

From the complex modulus $G^*(w)$ follow the *storage* and the *loss moduli*, $G'(w) = \mathrm{Re}(G^*(w))$ and $G''(w) = \mathrm{Im}(G^*(w))$, the *complex shear compliance* $J^*(w) = 1/G^*(w)$ as well as *storage* and the *loss compliances*, $J'(w) = \mathrm{Re}(J^*(w))$ and $J''(w) = -\mathrm{Im}(J^*(w))$. Furthermore, we also consider the *shear creep compliance* $J(t)$ (the response of the strain to a stress jump $t(t) = t_0\,Q(t)$), which is given here by

$$J(t) = \frac{E^{-1}}{G(1+b)}\left(\frac{t}{l}\right)^b . \tag{16}$$

As a direct consequence of the multiplication relation, equation (12), we can easily derive the harmonic response functions $G^*(w)$ and $J^*(w)$ of a given fractional RCE. On the other hand, the analytical evaluation of the step response functions, namely of $G(t)$ and $J(t)$, turns out to be a hard task in many cases. Nevertheless these responses can be derived explicitly for a whole series of fractional RCEs of practical importance, cf. sections 5 and 6.

3. HISTORICAL SURVEY OF RCEs WITH FRACTIONAL DERIVA-TIVES

To our knowledge, the mathematically sound use of fractional differentiation to describe rheological properties of materials starts with Gemant [28,29]. He modified the Maxwell model by introducing the semiderivative of the stress (i.e. $a = 1$ and $b = 1/2$ in equation (30), *vide infra*) in order to portray the properties of an 'elasto-viscous' fluid under oscillatory excitations. Nutting, on the other hand, pioneered power laws such as equation (1) to depict experimental results [30,31], although at that time the relation between power laws and fractional derivatives was not clear to the materials' science community. Other examples for the use of power laws are the works by P. Kobeko, E. Kuvshinskij and G. Gurevitch [32] (an expression used by them is equivalent to the Cole-Davidson function of dielectric relaxation) and by Alexandrov and Lazurkin [33]. There are even claims that stretched exponentials turn into power laws for exponents smaller than 0.4 [34], see, however also reference [7].

In rheology Scott-Blair et al. [35-38] made an extensive use of fractional integrodifferentiation to depict through power-laws the creep and relaxation in wide classes of materials. Their works rendered clear the intimate relationship between power laws and fractional calculus, and also introduced fractional generalizations of Newton's and Hooke's models, in which the fractional elements (FE) of this chapter were viewed as arising from 'quasi-properties', representing non-equilibrium states. Thus, in their notation, property X obeys generally an expression of the following type:

$$X \equiv \frac{d^a \boldsymbol{t}}{d\left(d^b \boldsymbol{g} / d\, t^b\right)^a} \quad . \tag{17}$$

Viewing τ as stress and γ as strain, the property X is an extension of the usual definition of viscosity, for which $\boldsymbol{a} = \boldsymbol{b} = 1$. Bosworth [39] made first considerations concerning the use of equation (17).

After these basic pioneering works, rheology experienced a renewed surge of activity on fractional calculus starting at the end of the '60ies. Thus Slonimsky [40] applied the calculus to study rheological phenomena of polymers, a materials' class of growing importance. He described by a fractional relation the force acting on a polymer segment and the displacement experienced by it; in fact the operator used by him can be represented as an infinite series of simple fractional derivatives. Then Smit and deVries [41] investigated several material functions, such as the complex shear modulus of the fractional Kelvin-Voigt model (having a fractional derivative of the strain) and compared the results with experimental data. Next, Meinardi and Caputo [20-22] developed the ideas of fractional calculus further; they provided expressions for several material functions for the fractional standard solid model (see below), for which the order of fractional differentiation was the same for the stress and the strain. The evaluation of the relaxation in this case was an important step towards the understanding of the basic properties of the whole class of fractional models. These results were not widely noticed, and later rederived in rheology by Friedrich [11-13] and Nonnenmacher [42-44], who also solved the general case, in which the two fractional derivatives are of different order. Meinardi and Caputo used their expressions [20-22] to describe relaxation measurements of rock materials, metals and glasses.

A study of the fractional versions of the Maxwell and Kelvin-Voigt models, where only the derivative of the stress was replaced by a fractional counterpart was performed by Koeller [45]. He also considered the generalization to parallel and serial arrangements, and also pointed out the close connection between the

Rabotnov calculus [46] and fractional integrodifferentiation. The Rabotnov calculus, developed in the USSR in the '60ies, is based on the Rabotnov-operator $\Re_{-a}^{-b}(f)$ (also called fractional-exponential operator), and was used widely for portraying relaxation phenomena in solid mechanics [46]. Friedrich and Hazanov poined out the relation between $\Re_{-a}^{-b}(f)$ and fractional integrodifferentiation [47]. One has namely:

$$\Re_{-a}^{-b}(f) = \sum_{k=1}^{\infty} (-b)^{k-1} \frac{d^{k(a-1)}f}{dt^{k(a-1)}} \quad \text{and} \quad \Re_{-a}^{0}(f) = \frac{d^{a-1}f}{dt^{a-1}} \tag{18}$$

where $0 \leq a < 1$ and $b \geq 0$.

More recently, one of the goals of research in our field was the detailed analysis of the fractional Maxwell and Kelvin-Voigt models. It was soon clear that the analytical determination of the response functions of these models is a mathematically difficult task (see below). Bagley and Torvik [48] connected the molecular theory of viscoelasticity to the fractional calculus, and showed that some aspects of the theory are mirrored by the fractional Kelvin-Voigt model. Friedrich and Heymann [15,16] pointed out the intimate relation between the order of differentiation in a fractional Kelvin-Voigt model and the degree of conversion for the sol-gel transition of a crosslinking polydimethylsiloxane.

Later, in 1986, Bagley and Torvik [49] considered the fractional standard solid model in more detail. They established that this model, which contains two fractional derivatives – one of the stress and one of the strain – is compatible with thermodynamics if the order of both derivatives is identical. Thermodynamical admissibility of fractional order models was also analyzed by Friedrich for several models [12].

In 1983, Rogers [50] formulated general RCEs containing a large number of sums or products of fractional derivatives, both of the stress and also of the strain. The analysis of these models was restricted to those containing mainly two fractional derivatives, and dealt with (the more accessible) frequency domain. Another use of fractional derivatives was put forward by VanArsdale who generalized the Rivlin-Ericksen and White-Metzner tensors by including fractional orders of differentiation [51].

Only in 1991 did Friedrich [11] as well as Glöckle and Nonnenmacher [42] succeed in obtaining $G(t)$ and $J(t)$ for the fractional Maxwell model containing two fractional derivatives of different order. They showed that this solution can be expressed through a special class of mathematical functions which will be discussed later in this Chapter. The derivation in references [44,52] is based on

an integral fractional representation of the standard solid model, whereas Friedrich's derivation uses the differential picture. Friedrich pointed out that the differential fractional version is thermodynamically admissible for wide ranges of parameters, whereas the parameter range of the fractional integral version is very restricted [17]. In subsequent works Glöckle and Nonnenmacher clarified the mathematical basis of fractional calculus by pointing out its relation to the so-called Fox-functions [42]. Moreover, they explained the interrelation between fractional relaxation functions and the time-temperature superposition principle [52]. We note that these models were successfully applied to the description of the viscoelastic properties of filled polymers [53].

In general, much of the very recent work is characterized by the search for the physical background underlying fractional calculus. The relation of this calculus to the classical spring-dashpot representation of complex viscoelastic materials is a central aspect of the works by Schiessel and Blumen [54-58], as well as by Heymans and Bauwens [59-61]. These works showed how power law relaxation follows from exemplary arrangements of springs and dashpots. Schiessel and Blumen succeeded in explaining the process of polymer cross-linking on the basis of such mechanical networks; they also investigated terminated ladder arrangements which mimic pre- and postgel behavior [56]. Such mechanical analogs also showed the way how physically reasonable fractional RCEs can be constructed, aspects discussed by Schiessel, Metzler, Blumen and Nonnenmacher [58] and by Heymans [61]. By employing a formal analogy between linear viscoelasticity and diffusion in a disordered structure Giona, Cerbelli and Roman derived a fractional equation describing relaxation phenomena in complex viscoelastic materials. This analogy leads to a power law expression, which is in agreement with the experimental results [62]. At the moment we are still far from being able to relate in a reductionistic way the empirical models to a microscopic background. Nevertheless, as will become evident in section 4 of this Chapter, the representation of fractional derivatives through spring-dashpot analogs is helpful in understanding a series of phenomena which underlie the fractional calculus formalism.

Another line of research, widely pursued nowadays, is the phenomenologically oriented, pragmatic modeling. An example for this is the work by Stastna, Zanzotto and Ho [63] who provided a relation between the Kobeko function [32] and fractional calculus and used it to model rheological data of asphalts. Stastna et al. found a general inversion scheme which generalizes Rogers' results [50]; it allows the representation of the complex shear modulus in the form:

$$G^*(w) = i h_0 w \left[\frac{\prod_{k=1}^{m} \left(1 + i w \, l_{1k} \right)}{\prod_{k=1}^{n} \left(1 + i w \, l_{2k} \right)} \right]^b . \tag{19}$$

In equation (19) λ_{1k} and λ_{2k} are two sets of characteristic times. The authors of reference [63] succeeded in deriving the corresponding fractional RCE. Note that for $m = 0$ and $n = 1$ one recovers the Kobeko function [24].

We close this section by noting that nowadays fractional calculus is of widespread use in describing different rheological phenomena for wide classes of materials. As examples from the polymer literature we refer to [19,53,64-67]. In the following section we analyze under which circumstances spring and dashpot arrangements lead to power law relaxations.

4. THE REPRESENTATION OF RCE WITH FRACTIONAL DERI-VATIVES BY MECHANICAL MODELS

Fractional RCEs may be formally derived from ordinary RCEs by replacing the first-order derivatives (d/dt) by fractional derivatives (d^β/dt^β) of non-integer order ($0 < \beta < 1$). This formal procedure can, however, not assure *a priori* that the resulting expressions are always physically reasonable. This aspect was pointed out, for instance, in references [11,42,54]. Thus it is useful to have a procedure at hand that automatically guarantees mechanical and thermodynamical stability.

As a first step Schiessel and Blumen [54-57] and Heymans and Bauwens [60] have demonstrated that the fractional relation, equation (4), can be realized physically through hierarchical arrangements of springs and dashpots, such as ladders, trees or fractal structures (which we will discuss in this section). The idea is that (disregarding for the moment the specific structure of the hierarchical constructions, these will be detailed later) equation (4) is obeyed by a *fractional element* (FE) which is specified by the triple (b, E, l). We symbolize the FE by a triangle, as shown it Figure 3(c), where also its classical counterparts are depicted: the spring (cf. Figure 3(a)) obeying equation (5) and the dashpot (cf. Figure 3(b)) with the stress-strain relationship equation (6). Then, as a second step, more complicated RCEs can be constructed by combining two or more FEs in serial, parallel or more complex arrangements; this was proposed by Schiessel et al. [58] and by Heymans [61]. We will make use of this method in sections 5 and 6.
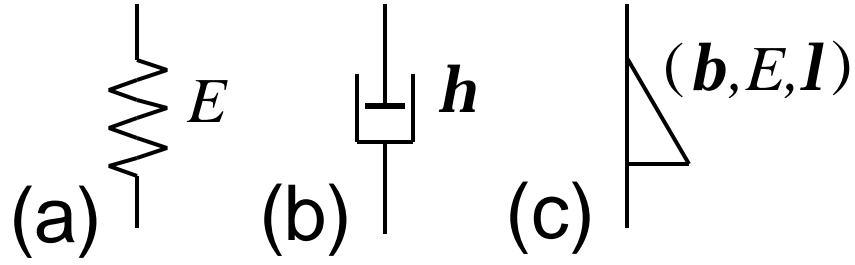
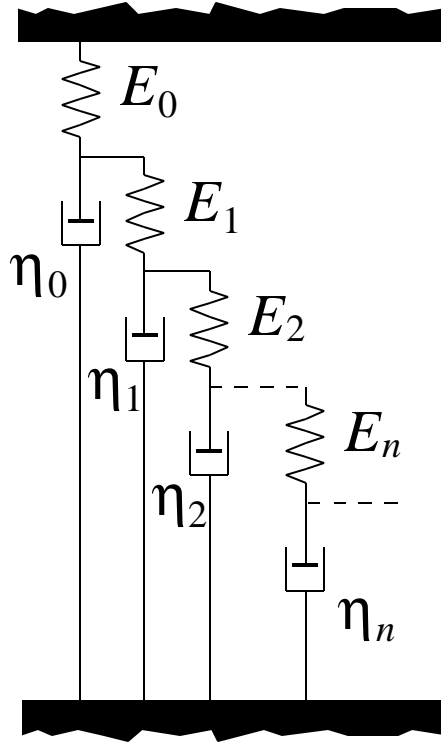Figure 3. Single elements: (a) elastic, (b) viscous and (c) fractional.

Figure 4. A sequential spring-dashpot realization of the fractional element.

Let us now consider different realizations of FEs. In reference [54] Schiessel and Blumen proposed a ladder-like structure with springs (having spring constants E_0, E_1, E_2,...) along one of the struts and dashpots (with viscosities h_0, h_1, h_2,...) on the rungs of the ladder (cf. Figure 4). As shown in reference [54] the complex modulus $G^*(w)$ admits a continued fraction expression, namely

$$G^*(w) = \frac{E_0}{1+} \quad \frac{(iw)^{-1}\frac{E_0}{h_0}}{1+} \quad \frac{(iw)^{-1}\frac{E_1}{h_0}}{1+} \quad \frac{(iw)^{-1}\frac{E_1}{h_1}}{1+}..., \tag{20}$$

where we use a standard notation for continued fractions, $\left[a/(b+) \right] f = a/(b+f)$, cf. reference (23). Choosing in equation (20) $E_0 = E_1 = \ldots = E$ and $\boldsymbol{h}_0 = \boldsymbol{h}_1 = \ldots = \boldsymbol{h}$ it can be shown (by comparing terminating approximations of the continued fraction with the binomial series) that the complex modulus of the infinite arrangement is given by

$$G^*(\boldsymbol{w}) = E \frac{(4(i\boldsymbol{wl})^{-1} + 1)^{1/2} - 1}{2(i\boldsymbol{wl})^{-1}} \tag{21}$$

where we set $\lambda = \eta/E$. For $\boldsymbol{wl} \ll 1$ equation (21) reduces to the form $G^*(\boldsymbol{w}) \cong E(i\boldsymbol{wl})^{1/2}$. Therefore having the same spring constants and viscosities for the whole arrangement one gets a complex modulus with $\beta = 1/2$, and thus the ladder model with equal springs and dashpots leads to a FE with the parameters $(1/2, E, \boldsymbol{l})$. To extend the ladder model to arbitrary values of β with $0 < \beta < 1$, a suitable distribution for the spring constants and viscosities has to be chosen; thus an algebraic k-dependence of the material constants of the form

$$E_k \propto \eta_k \propto k^{1-2\beta} \tag{22}$$

leads to a FE specified by $(\boldsymbol{b}, E, \boldsymbol{l})$ [54].
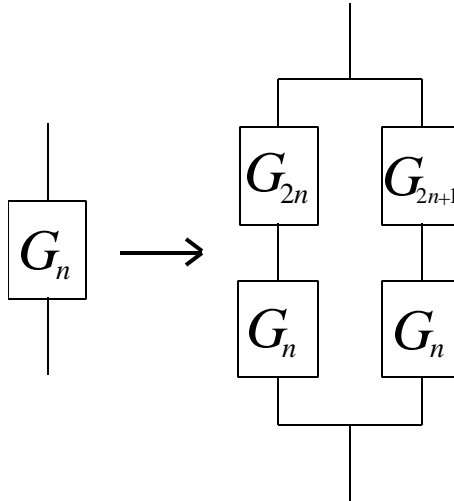

Figure 5. Recursive construction of the iterated mechanical networks of Heymans and Bauwens [60].

Heymans and Bauwens [60] and Schiessel and Blumen [56] demonstrated that values of β with $\beta \neq 1/2$ can also be attained by arranging equal springs and dashpots into a network with a more complex structure. Thus reference [60] focuses on a class of iterated networks which are generalizations of a fractal tree model; each FE (b, E, l) can be represented by such an arrangement to any desired accuracy. We show in Figure 5 the recursive construction of the model: One starts from an element having the complex modulus G_1; this element gets then represented by four elements, two of which have G_1, the two others G_2 and G_3 as moduli (cf. Figure 5 with $n = 1$) so that the ensuing structure still has G_1 as complex modulus. From Figure 5 it is easily seen that the relation between the complex moduli of the elements has to be $G_n = \sqrt{G_{2n} G_{2n+1}}$. In principle the iteration proceeds for each element indefinitely. By this the complex modulus G_1 of the whole arrangement is

$$G_1 = (G_2 G_3)^{1/2} = (G_4 G_5 G_6 G_7)^{1/4} = ... \prod_{k=2^n}^{2^{n+1}-1} (G_k)^{1/2^n} \tag{23}$$

At each level n of decomposition one replaces some of the elements G_k ($k = 2^n, ..., 2^{n+1} - 1$) by either purely elastic elements, i.e. springs with spring constant E, or purely viscous elements, i.e. dashpots with viscosity η. For these elements one has to replace G_k in equation (23) by E or iwh and stop their further decomposition. Let N_n denote the number of springs at the nth level of decomposition and M_n the corresponding number of dashpots. From equation (23) it follows:

$$G_1 = E^{\Sigma N_n/2^n} (iwh)^{\Sigma M_n/2^n} = E(iwl)^b \tag{24}$$

with $b = \sum_n M_n/2^n$ and $l = h/E$. Thus one can reach any preset, arbitrary β, $0 < \beta < 1$ to any desired accuracy by a sufficiently fine decomposition. As a special case, by taking $G_2 = E$ and $G_3 = iwh$ we obtain a binary tree. This network, which we depict in Figure 6, is again a FE with the parameters $(1/2, E, l)$.
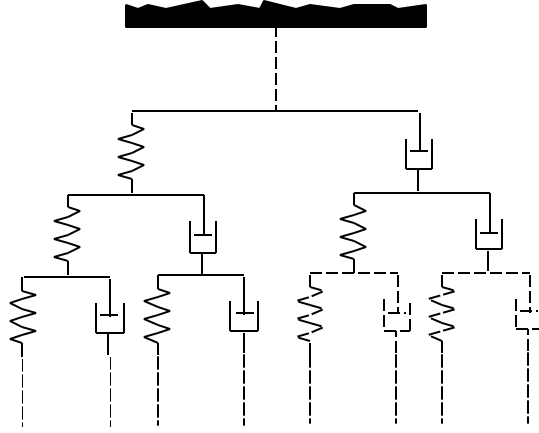
14

Figure 6. A special case of the iterated networks shown in Figure 5: binary spring-dashpot tree.

The advantage of the "binary decomposition" of elastic and viscous elements is its simple analytical tractability; in many cases, however, it leads to complicated networks whose properties are difficult to grasp intuitively. Thus it is also desirable to work with networks whose structural properties (such as the connectivity) and the exponent β are related in a more obvious fashion.

In reference [56] Schiessel and Blumen showed that for given fractal networks this relation is straightforward when the springs and dashpots are suitably chosen. The construction starts by connecting each site $\mathbf{r}_i$ of the given network to neighboring nodes $\mathbf{r}_j$ by equal springs (with spring constant E) and linking each $\mathbf{r}_i$ to the ground via a site-dependent dashpot (with viscosity $\boldsymbol{h}_i = z(\mathbf{r}_i)\boldsymbol{h}$, where $z(\mathbf{r})$ is the coordination number of node $\mathbf{r}_i$). Furthermore, the nodes' motion is perpendicular to the ground. To give an example we show in Figure 7 a section of the infinite mechanical network constructed from the Sierpinski gasket. The analogy to random walks can now be seen by comparing the stresses acting on node $\mathbf{r}_i$ (whose displacement is γ_i)

$$\boldsymbol{h}_i \dot{\boldsymbol{g}}_i(t) = E \sum_{j(i)} \left[\boldsymbol{g}_j(t) - \boldsymbol{g}_i(t) \right] \tag{25}$$

with the master equation

$$\frac{dP(\mathbf{r}_i,t)}{dt} = \sum_{j(i)} \left[w_{ij} P(\mathbf{r}_j,t) - w_{ji} P(\mathbf{r}_i,t) \right] \tag{26}$$

15

which governs the probability $P(\mathbf{r}_i, t)$ of having a random walker at site $\mathbf{r}_i$. In Eqs. (25) and (26) the sums run over all nearest neighbors $\mathbf{r}_j$ of $\mathbf{r}_i$. The transition probabilities w_{ij} in Eq. (26) obey $z(\mathbf{r}_j)w_{ij} = w = \text{constant}$. Now one can identify formally $\boldsymbol{h}_i \boldsymbol{g}_i(t)$ with $P(\mathbf{r}_i, t)$. Furthermore, the probability for a random walker to return to the origin at time t follows an algebraic form:

$$P(t) \propto t^{-d_s/2} \tag{27}$$

where d_s is the spectral dimension of the network [68]. A power law behavior of the complex modulus, Eq. (15), follows, with $\beta = 1 - d_s/2$ (cf. Ref. [56] for details). The ladder model, Figure 2, is the special case of a one-dimensional lattice with $d_s = 1$ and thus $\beta = 1/2$; the Sierpinski gasket in 2d (cf. Figure 7) has $d_s = 2\ln(3)/\ln(5)$ and hence $\boldsymbol{b} = 1 - \ln(3)/\ln(5) \cong 0.317$.
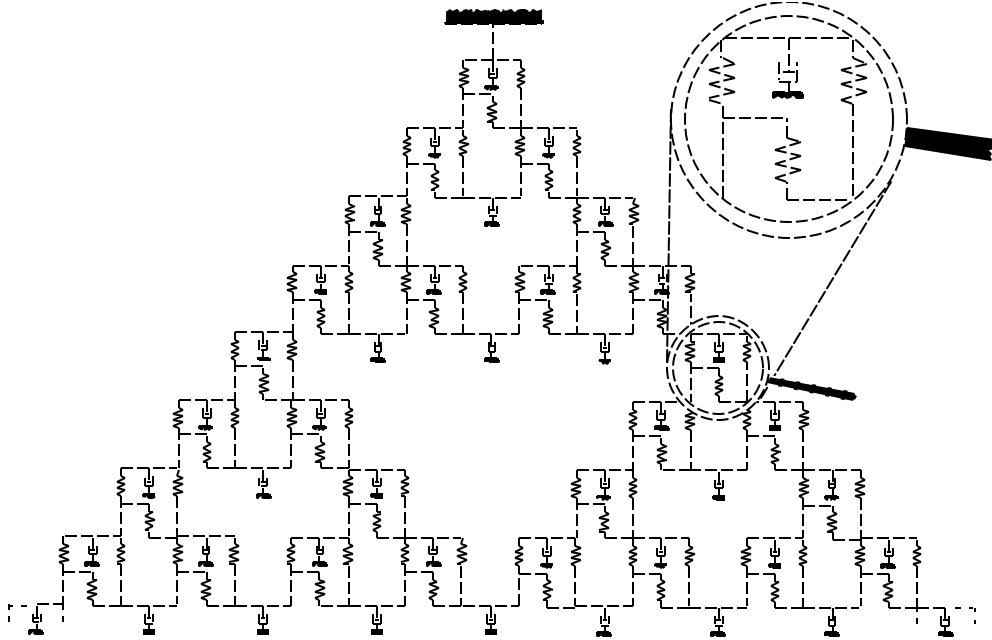

Figure 7. Section of the infinite spring-dashpot arrangement based on the Sierpinki gasket.

An interpretation of the sol-gel transition in terms of such mechanical networks can be found in Ref. [56].

5. FRACTIONAL MAXWELL AND KELVIN-VOIGT MODELS

Figure 8(a) shows the standard Maxwell model, in which a spring and a dashpot are arranged in series [24,25]. Now this model can be generalized by replacing these elements by the FEs $(\boldsymbol{a}, E_1, \boldsymbol{l}_1)$ and $(\boldsymbol{b}, E_2, \boldsymbol{l}_2)$, as shown in Figure 8(b). Due to the sequential construction the stress $\boldsymbol{t}(t)$ is the same for both elements. Their respective stress-strain relations are

$$\boldsymbol{g}_1(t) = E_1^{-1} \boldsymbol{l}_1^{-a} \frac{d^{-a} \boldsymbol{t}(t)}{dt^{-a}}, \quad \boldsymbol{g}_2(t) = E_2^{-1} \boldsymbol{l}_2^{-b} \frac{d^{-b} \boldsymbol{t}(t)}{dt^{-b}} \tag{28}$$

where both expressions follow from the composition rule, Eq. (10). Due to the sequential construction of the fractional Maxwell model (FMM), we have $\boldsymbol{g}(t) = \boldsymbol{g}_1(t) + \boldsymbol{g}_2(t)$, from which it follows that

$$\boldsymbol{t}(t) + \frac{E_1 \boldsymbol{l}_1^a}{E_2 \boldsymbol{l}_2^b} \frac{d^{a-b} \boldsymbol{t}(t)}{dt^{a-b}} = E_1 \boldsymbol{l}_1^a \frac{d^a \boldsymbol{g}(t)}{dt^a} \quad . \tag{29}$$

Let us assume without loss of generality that $\alpha > \beta$. Eq. (29) can be further simplified by setting $\boldsymbol{l} = \left(E_1 \boldsymbol{l}_1^a / E_2 \boldsymbol{l}_2^b \right)^{1/(a-b)}$ and $E = E_1 (\boldsymbol{l}_1/\boldsymbol{l})^a$. This leads to

$$\boldsymbol{t}(t) + \boldsymbol{l}^{a-b} \frac{d^{a-b} \boldsymbol{t}(t)}{dt^{a-b}} = E \boldsymbol{l}^a \frac{d^a \boldsymbol{g}(t)}{dt^a} \tag{30}$$

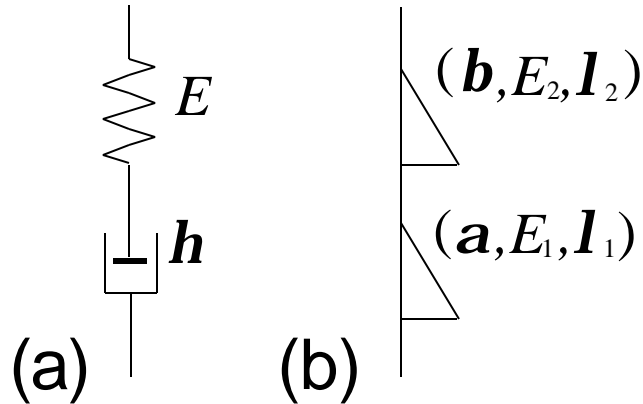which is the RCE of the FMM [11,43,58].

Figure 8. The (a) ordinary and (b) the fractional Maxwell model

When one arranges the spring and the dashpot in parallel one obtains the standard Kelvin-Voigt model [24,25], depicted in Figure 9(a). Its generalization, which has two FEs, is shown in Figure 9(b). Because of the parallel arrangement, the stresses acting on the two elements are additive. Following a procedure similar to that for the generalized Maxwell model (*vide supra*), one finds for the RCE of the generalized Kelvin-Voigt model (FKVM) [58]

$$t(t) = E\boldsymbol{l}^a \frac{d^a \boldsymbol{g}(t)}{dt^a} + E\boldsymbol{l}^b \frac{d^b \boldsymbol{g}(t)}{dt^b} \tag{31}$$

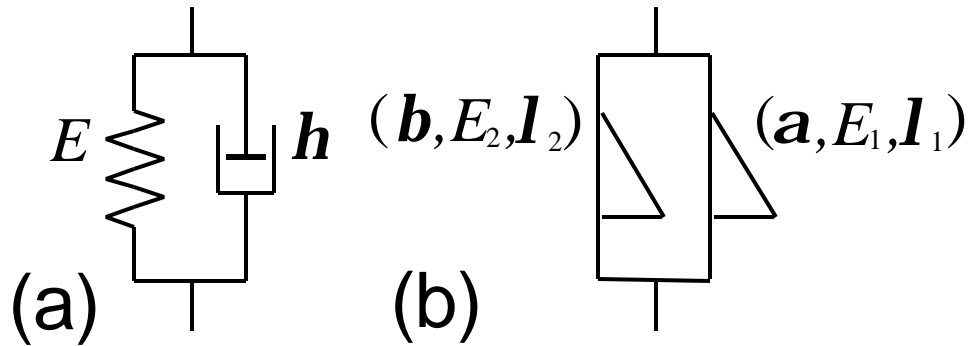where we have used the same parameters λ and E as for the FMM.

Figure 9. (a) The Kelvin-Voigt model and (b) its fractional generalization.

The basic material functions of the FMM and the FKVM were derived elsewere [58]; we will restrict ourselves to their succinct display and to the discussion of their basic properties. Table 1 presents for both models their fundamental response functions.

Table 1
Material functions of the fractional Maxwell and Kelvin-Voigt models

	FMM		FKVM	
$G(t)$	$E\left(t/l\right)^{-b}E_{a-b,1-b}\left(-(t/l)^{a-b}\right)$	(32)	$\dfrac{E}{G(1-a)}\left(\dfrac{t}{l}\right)^{-a}+\dfrac{E}{G(1-b)}\left(\dfrac{t}{l}\right)^{-b}$	(33)
$J(t)$	$\dfrac{E^{-1}}{G(1+a)}\left(\dfrac{t}{l}\right)^{a}+\dfrac{E^{-1}}{G(1+b)}\left(\dfrac{t}{l}\right)^{b}$	(34)	$E^{-1}\left(t/l\right)^{a}E_{a-b,1+a}\left(-(t/l)^{a-b}\right)$	(35)
$G^{*}(w)$	$E\,\dfrac{\left(iwl\right)^{a}}{1+\left(iwl\right)^{a-b}}$	(36)	$E\left(iwl\right)^{a}+E\left(iwl\right)^{b}$	(37)
$J^{*}(w)$	$E^{-1}\left(iwl\right)^{-a}+E^{-1}\left(iwl\right)^{-b}$	(38)	$E^{-1}\,\dfrac{\left(iwl\right)^{-b}}{1+\left(iwl\right)^{a-b}}$	(39)

In Table 1 $E_{a,b}(z)$ denotes the generalized Mittag-Leffler function of argument z, whose definition and basic properties are given in the Appendix. This function is of great importance for fractional RCEs, since it occurs in many material functions in the time domain. The harmonic response functions, equations (36) to (39), follow simply from the RCEs, equations (30) and (31), by means of the multiplication rule, equation (12). Due to the sequential (parallel) construction of the FEs in the FMM (FKVM), the response $J(t)$ ($G(t)$) is simply the sum of the corresponding responses of its structural parts, which obey equation (16) (equation (1)).
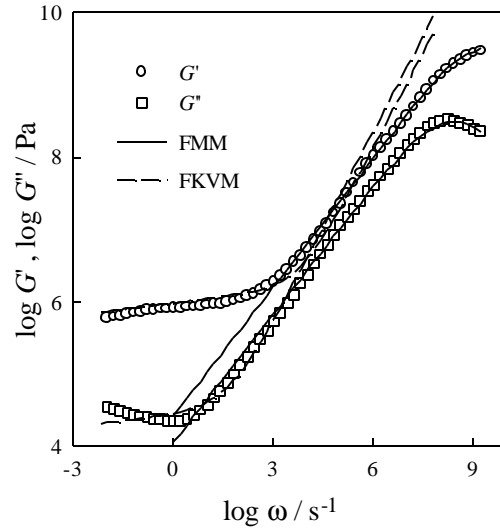
Figure 10. Description of the data of Figure 1(a) by the fractional Maxwell model (solid lines) and the fractional Kelvin-Voigt model (dashed lines).

Table 2
Material parameters used in Figure 10

	log E	log λ	α	β
FMM	9.09	-8.36	0.583	0.593
FKVM	5.75	-2.96	0.057	0.885

Using the asymptotic expansions of the Mittag-Leffler function and focussing on the behavior of the dynamic moduli and of the dynamic compliances it becomes clear that both the FMM and the FKVM describe two power law regions which intersect each other at the characteristic time $t = 1$. In the case of the relaxation function $G(t)$ the FMM describes first a flat decrease (of slope $-b$) followed by a steeper decrease (of slope $-a$), whereas for the FKVM the flat decrease follows the steeper decrease. The compliance of the FMM shows a flat increase with slope β followed by a steeper increase with slope α; for the FKVM the situation is reversed.

Thus it follows that in the time domain the FMM can be used to describe relaxation functions which start from a plateau region and decrease according to power laws, whereas the FKVM is able to describe the relaxation via a power law to a plateau. The situation is correspondingly reversed in the frequency domain. Note, however, that a so-called S-shaped transition between two plateaus which

are connected by a power law cannot be described by means of FMM or of FKVM.

An example for the use of FMM is presented in Figure 10, in which the dynamic moduli of polyisobutylene are redrawn from Figure 1(a). These are compared to the results of FMM with the parameters given in Table 2. Note the good agreement between the experimental data and the analytical expressions for FMM. On the other hand FKVM is unable to describe the observed features even qualitatively. This is especially true for the $G''(\omega)$ data where FKVM can not follow the decline found experimentally in the range of very low frequencies.

In Figure 11 (which is redrawn from Figure 2) we provide another example which stresses the possibilities offered by FMM to depict relaxation data. Whereas Figure 1 is concerned with polymers in the glassy and transitional zones, here we deal with relaxation from the plateau towards the terminal relaxation zone. Figure 11 shows the storage moduli, both of two modified polybutadienes (PB302 and PB304) and also of the neat polymer, on which the modifications were performed (PB300) [64]. Note that the FMM with the parameters given in Table 3 describes in a quantitative way the observed relaxation – the focus lies here on the power law behavior of the modified PBs at very low frequencies. We note furthermore that both the storage and the loss module of the neat polymer melt are quantitatively depicted by this model. The same holds true for polystyrene, as shown in the following example, taken from reference [65]. The situation is depicted in Figure 12; as is obvious, the storage moduli of polystyrene filled with different amounts of silicagel (N20) follow a power law in an intermediate region. Here the slope of the low frequency plateau is zero; consequently the system can be modeled by adding a Hookean spring (of strength G_e) in parallel to the two FEs. The agreement between this model and the experimental data is very good. The Ulm group [44,53] used a similar model (the integral version of the FMM) to describe the complex moduli of filled polymers.

On the other hand, the example of Figure 12 demonstrates the need to go to models having more than two FEs in order to describe more complex behavior patterns, such as S-shaped transitions. Such extensions are the focus of the next section.
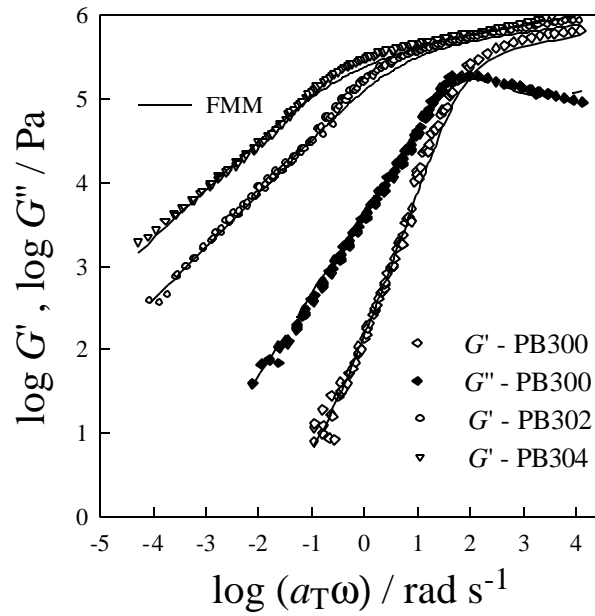
Figure 11. Description of the data of Figure 2 by the fractional Maxwell model (solid lines).

Table 3
Material parameters used in Figure 11

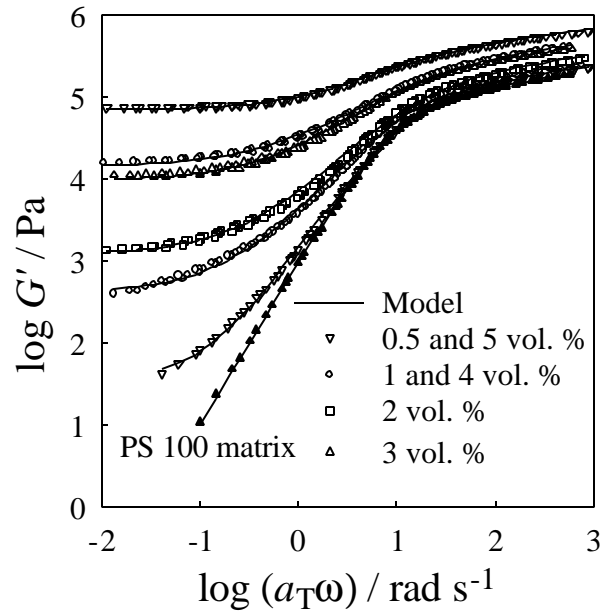|	log E	log λ	α	β
PB300	5.52	-1.87	0.882	0.994
PB302	5.60	-0.344	0.553	0.632
PB304	5.48	0.720	0.478	0.590

Figure 12. Storage modulus $G'(a_T w)$ for aerosil-filled polystyrene. The solid lines give the description through the fractional Maxwell model. The aerosil concentration increases from below.

Table 4
Material parameters used in Figure 12

	log E	log λ	α	β	log G_e
PS100	4.97	-0.877	0.812	1.000	$-\infty$
0.5 vol. %	5.07	-1.06	0.808	0.988	1.54
1 vol. %	5.17	-1.08	0.749	0.907	2.62
2 vol. %	5.26	-1.12	0.718	0.867	3.09
3 vol. %	5.40	-1.03	0.649	0.784	3.99
4 vol. %	5.47	-1.15	0.597	0.725	4.15
5 vol. %	5.49	-0.814	0.613	0.768	4.85

6. MORE COMPLEX MODELS

6.1 Models based on combinations of 3 fractional elements

Here we present more complex models, which are combinations of three FEs. We dispense with considering the fully parallel or the fully linear combination of FEs. We view as much more interesting the parallel arrangement of the FMM with a third FE or the sequential combination of the fractional Kelvin-Voigt model with a third FE. We call these models the fractional Zener model (FZM, also fractional standard solid model) and the fractional Poynting-Thomson model (FPTM), respectively. We stop to note that Heymans [61] has also analyzed more complex models, which are composed of FEs and additional conventional elements.

The constitutive equations of FZM and of FPTM (these being our basic, simplest models containing 3 FEs) can be derived along the lines of the previous section.
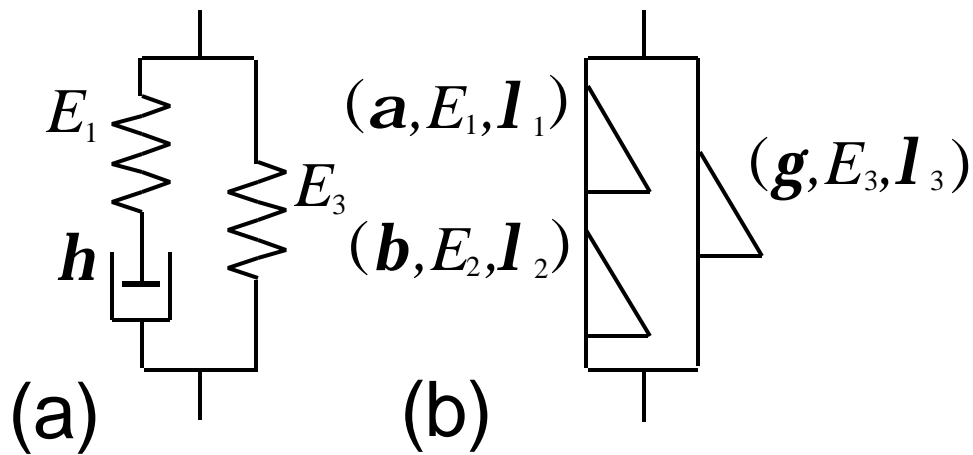

Figure 13. The (a) ordinary and (b) fractional Zener model.

We start with the analysis of the FZM. The mechanical representation of the FZM is displayed in Figure 13; it consists of an FMM (with the same parameters as in Figure 8) in parallel to an FE specified by (g, E_3, l_3). The stresses on the left and right branches of the arrangement, τ_L and τ_R, obey the following stress-strain-relationships:

$$t_L(t) + l^{a-b} \frac{d^{a-b} t_L(t)}{dt^{a-b}} = E l^a \frac{d^a g(t)}{dt^a} \quad , \tag{40}$$

cf. equation (30) and, equation (4),

$$t_R(t) = E_3 \mathbf{1}_3^g \frac{d^g \mathbf{g}(t)}{dt^g} \quad .$$ (41)

Both stresses add, which leads to the RCE of the FZM:

$$t(t) + \mathbf{1}^{a-b} \frac{d^{a-b} t(t)}{dt^{a-b}} = E\mathbf{1}^a \frac{d^a \mathbf{g}(t)}{dt^a} + E_0 \mathbf{1}^g \frac{d^g \mathbf{g}(t)}{dt^g} + E_0 \mathbf{1}^{g+a-b} \frac{d^{g+a-b} \mathbf{g}(t)}{dt^{g+a-b}}$$ (42)

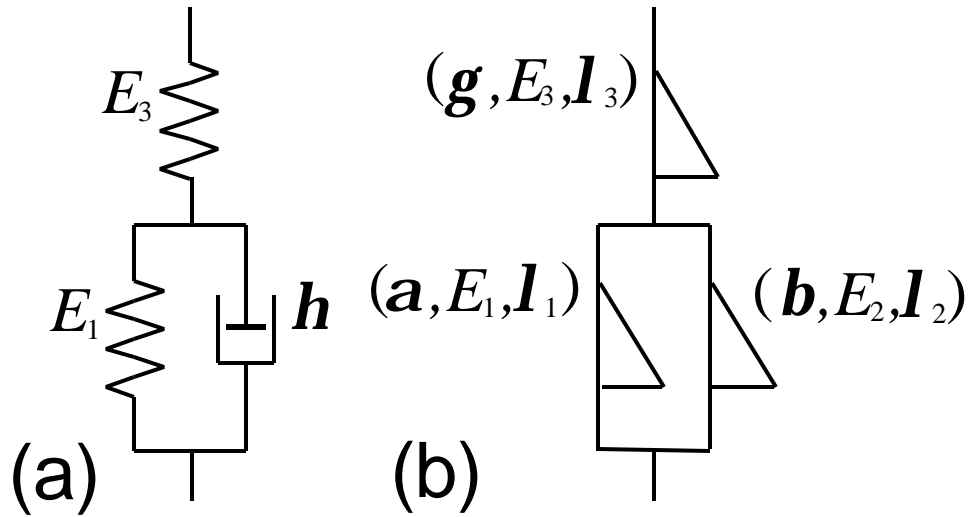Here we set $E_0 = E_3 (\mathbf{1}_3 / \mathbf{1})^g$.

Figure 14. The (a) Poynting-Thomson model and (b) its fractional generalization.

The FPTM consists of a serial arrangement of the FKVM (with the same parameters as in Figure 9) and an FE $(\mathbf{g}, E_3, \mathbf{1}_3)$ (cf. Figure 14). The RCE of this arrangement can be derived by noting that the deformations of the Kelvin-Voigt element and of the FE simply add, which leads to:

$$t(t) + \frac{E}{E_0} \mathbf{1}^{a-g} \frac{d^{a-g} t(t)}{dt^{a-g}} + \frac{E}{E_0} \mathbf{1}^{b-g} \frac{d^{b-g} t(t)}{dt^{b-g}} = E\mathbf{1}^a \frac{d^a \mathbf{g}(t)}{dt^a} + E\mathbf{1}^b \frac{d^b \mathbf{g}(t)}{dt^b}$$ (43)

where we again set $E_0 = E_3 \left(\mathbf{1}_3 / \mathbf{1} \right)^g$.

We again summarize (now in Table 5) the relaxation material functions of the two models. For the detailed derivation of the expressions given in the Table we refer the reader to [58]. Here we note only that the dynamic moduli as well as the dynamic compliances follow directly from the corresponding RCEs by means of the multiplication rule, equation (12). Moreover, the relaxation modulus (creep compliance) of the FZM (FPTM) is simply the sum of the moduli (compliances) of the corresponding substructures. On the other hand, the creep compliance (relaxation modulus) of the FZM (FPTM) is only known analytically for the special cases $\gamma = \alpha$ or $\gamma = \beta$, cf. [58]; in Table 5 the case $\gamma = \beta$ is presented. The constants C_1 and C_2 of Table 5 are $C_1 = \left(E_0 / (E + E_0) \right)^{1/(a-b)}$ and $C_2 = \left(E / (E + E_0) \right)^{1/(a-b)}$.

Table 5
Material functions of the fractional Zener and the Pointing-Thomson models

	FZM		FPTM	
$G(t)$	$G_{\mathrm{FMM}}(t) + G_{\mathrm{FE}}(t)$	(44)	$\left(\dfrac{E_0}{E} \right)^2 C_2^{\alpha - 2\beta} G_{\mathrm{FMM}}(C_2^{-1} t)$ $+ \dfrac{E}{E + E_0} G_{\mathrm{FE}}(t), \quad \text{for } \gamma = \beta$	(45)
$J(t)$	$\left(\dfrac{E}{E_0} \right)^2 C_1^{\alpha - 2\beta} J_{\mathrm{FKVM}}(C_1 t)$ $+ \dfrac{E_0}{E + E_0} J_{\mathrm{FE}}(t), \quad \text{for } \gamma = \beta$	(46)	$J_{\mathrm{FKVM}}(t) + J_{\mathrm{FE}}(t)$	(47)
$G^*(\mathbf{w})$	$G_{\mathrm{FMM}}^*(\mathbf{w}) + E_0 (i \mathbf{w} \mathbf{l})^g$	(48)	$\dfrac{(i \mathbf{w} \mathbf{l})^a + (i \mathbf{w} \mathbf{l})^b}{E^{-1} + E_0^{-1} (i \mathbf{w} \mathbf{l})^{a-g} + E_0^{-1} (i \mathbf{w} \mathbf{l})^{b-g}}$	(49)
$J^*(\mathbf{w})$	$\dfrac{(i \omega \lambda)^{-\alpha} + (i \omega \lambda)^{-\beta}}{E + E_0 (i \omega \lambda)^{\gamma - \alpha} + E_0 (i \omega \lambda)^{\gamma - \beta}}$	(50)	$J_{\mathrm{FKVM}}^*(\mathbf{w}) + E_0^{-1} (i \mathbf{w} \mathbf{l})^{-g}$	(51)

The FZM can describe S-shaped transitions from one plateau to another via a power law. For instance, it can be shown [58] that $G(t)$ displays three regimes for $0 \leq g \leq b < a$ and $E \gg E_0$:

$$G(t) \propto \begin{cases} t^{-\beta} & \text{for } t \ll \lambda \\ t^{-\alpha} & \text{for } \lambda \ll t \ll \lambda_1 \\ t^{-\gamma} & \text{for } \lambda_1 \ll t . \end{cases} \qquad (52)$$

where $\lambda_1 \approx \left(E/E_0\right)^{1/(\alpha-\gamma)} \lambda$. In section 5 we have already presented an example where the FZM fits experimental data very well for the special case $\gamma = 0$ (cf. Figure 12).

6.2 Other models

Another approach which extends the use of FE-based models is pragmatic. The previous sections dealt with the exact solutions (relaxation functions) of models created by combining an increasing number of FEs in parallel and/or in series. The approach which we discuss here is the direct empirical modification (based on experimental findings) of the basic relaxation functions of the FE models. We now provide examples taken from the literature for such modifications.

6.2.1 Modification of the relaxation function

As already mentioned (see Figure 2) the $G'(\omega)$ and $G''(\omega)$ of monodisperse linear polymers show a sharp transition from a $G' \propto w^2$, $G'' \propto w$ behavior to a $G' \propto w^a$, $G'' \propto w^{-b}$ behavior. In the example of Figure 2 $\beta \cong 1/4$ and α is positive and close to zero, hence G' displays a quasi-plateau. In the corresponding relaxation experiment the stress decays then first according to a power law with slope $-a$, which is followed by an exponential relaxation at longer times. Figure 15 shows the relaxation function $G(t)$ of a modified polybutadiene [64] where the appearance of an intermediate power-law domain is clearly evident. In Figure 15, due to experimental limitations, the plateau can not be seen directly but it can be infered from its dynamic modulus (especially from the range $a_T w > 10$), displayed in Figure 16. Now, fluid behavior is associated with the termination of all relaxation processes, say at the time λ_m, and thus λ_m is a natural cut-off. This can be achieved phenomenologically by multiplying the

corresponding decay function with an exponential. As an example, starting from $G_{FMM}(t)$ (cf. equation (32)) in reference [18] the following 6-parameter relaxation function was put forward

$$G(t) = G_0 \, (t/\boldsymbol{l})^{\boldsymbol{a}-\boldsymbol{b}} \, E_{\boldsymbol{a},\boldsymbol{a}-\boldsymbol{b}+1}\!\left(-(t/\boldsymbol{l})^{\boldsymbol{a}}\right) \quad \exp(-t/\boldsymbol{l}_m) \; . \tag{53}$$

In equation (53) G_0 is a constant, $\boldsymbol{l}$ and $\boldsymbol{l}_m$ are time constants (with $\boldsymbol{l}_m \gg \boldsymbol{l}$) and $E_{\boldsymbol{a},\boldsymbol{a}-\boldsymbol{b}+1}$ denotes the generalized Mittag-Leffler function (α and β are related to the parameters $\boldsymbol{a}_{FMM}$ and $\boldsymbol{b}_{FMM}$ of equation (32) via $\boldsymbol{a} = \boldsymbol{a}_{FMM} - \boldsymbol{b}_{FMM}$ and $\boldsymbol{b} = \boldsymbol{a}_{FMM}$). From the asymptotic expansion of the Mittag-Leffler function for $\boldsymbol{b} < 1$ it follows that for $t \ll \lambda$ (plateau regime) $G(t) \propto t^{\alpha-\beta}$ and for $\lambda \ll t \ll \lambda_m$ (intermediate regime) $G(t) \propto t^{-\boldsymbol{b}}$. Moreover, thermodynamic stability requires that the power law exponents obey $0 < \boldsymbol{a} \le \boldsymbol{b} \le 1$. The cut-off function, $\exp(-t/\boldsymbol{l}_m)$, guarantees the fast release of stresses for $t > \boldsymbol{l}_m$ and hence induces a fluid-type behavior. A detailed discussion of this model is given in references [10] and [18]. We only provide here the main formulae.

Thus the dynamic moduli associated with equation (53) are

$$G^*(\boldsymbol{w}) = G_0 \, i\boldsymbol{w}\boldsymbol{l} \; \frac{\left(i\boldsymbol{w}\boldsymbol{l} + 1/\boldsymbol{l}_m\right)^{\boldsymbol{b}-1}}{1 + \left(i\boldsymbol{w}\boldsymbol{l} + 1/\boldsymbol{l}_m\right)^{\boldsymbol{a}}} \tag{54}$$

and

$$J^*(\boldsymbol{w}) = \frac{1 + \left(i\boldsymbol{w}\boldsymbol{l} + 1/\boldsymbol{l}_m\right)^{\boldsymbol{a}}}{G_0 \, i\boldsymbol{w}\boldsymbol{l} \, \left(i\boldsymbol{w}\boldsymbol{l} + 1/\boldsymbol{l}_m\right)^{\boldsymbol{b}-1}} \; . \tag{55}$$

Especially the dynamic moduli turn out to be particularly useful, since they lead to equations which are easy to use for fits to the data. Figure 16 shows exemplarily both the data and the obtained fits. For the PB202 sample we obtain $\boldsymbol{b} = 0.578$ and $\log \boldsymbol{l}_m = 2.48$. This is in good agreement with the parameters $\boldsymbol{b} = 0.556$ and $\log \boldsymbol{l}_m = 2.24$ which are determined by fitting equation (53) to the relaxation function of the sample displayed in Figure 15.

In Figure 15 the glassy short-time behavior (with the plateau modulus G_0) is not in the experimentally accessible range. In such a case the data may be fitted by a simpler relaxation function, which one obtains from equation (53) by letting $\boldsymbol{l} \to 0$. This leads to

$$G(t) = G_{01} \cdot (t/\lambda_m)^{-b} \exp(-t/\lambda_m) \qquad (56)$$

with $G_{01} = \eta_0/\lambda_m$, where η_0 is the zero-shear viscosity, $\eta_0 = \int_0^\infty G(t)dt$. Equation (56) is an empirical relaxation function of widespread use; thus its dynamic moduli were often used in fitting data (cf. reference [24]).
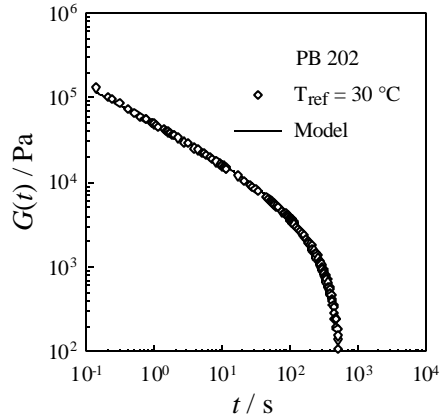

Figure 15. Relaxation function $G(t)$ of a modified polybutadiene (PB 202, M_W = 21 kg/mol). The solid line is equation (56) with log G_{01} = 4.68 Pa, log λ_m = 2.24 s and β = 0.556.
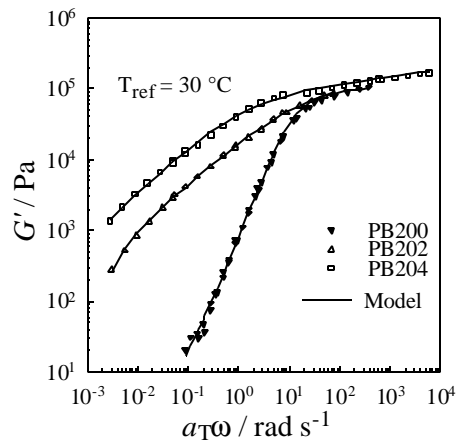

Figure 16. Storage modulus $G'(a_T\omega)$ for unmodified (PB200) and modified (PB202 and PB204) polybutadiene. The solid lines represent the fit of the generalized fractional Maxwell model according to equation (54) to the data.

As another example we present in Figure 17 the dynamic moduli of a partly cross-linked polybutadiene, PB 18, in the pregel stadium [9,69]. PB 18 is a polymer with a branched structure; it is gratifying to note that also in this case fractional relaxation provides a very good description of the experimental observations.
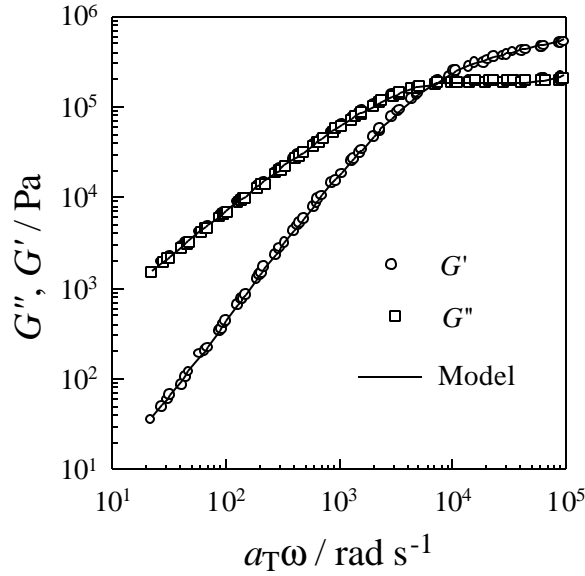

Figure 17. Storage $G'(a_T w)$ and loss modulus $G''(a_T w)$ for polybutadiene (PB18), for details see reference [69]. The solid lines represent the fit of the generalized fractional Maxwell model according to equation (54) to the data.

Let us now turn to the RCE associated with the relaxation function, equation (53). Starting from equation (54) it can be shown by means of the multiplication rule, equation (12), that the RCE has the following form [10]:

$$\tau(t) + \lambda^\alpha e^{-t/\lambda_m} \frac{d^\alpha}{dt^\alpha}\left[e^{t/\lambda_m} \tau(t)\right] = G_0 \lambda^\beta \; e^{-t/\lambda_m} \frac{d^{\beta-1}}{dt^{\beta-1}}\left[e^{t/\lambda_m} \frac{d\gamma(t)}{dt}\right] . \tag{57}$$

Equation (57) contains an explicit time dependence that can be removed using the product rule for fractional differential operators (cf. equation (5.5.2) of [26]). In this way, the RCE, equation (57) takes the form [10]:

$$t(t) + w^{\boldsymbol{a}} \sum_{i=0}^{\infty} \binom{\boldsymbol{a}}{j} \boldsymbol{l}_m^{a_i} \frac{d^{a_i} \boldsymbol{t}(t)}{dt^{a_i}} = G_0\, w^{\boldsymbol{b}} \sum_{j=0}^{\infty} \binom{\boldsymbol{b}-1}{j} \boldsymbol{l}_m^{b_j} \frac{d^{b_j} \boldsymbol{g}(t)}{dt^{b_j}} \qquad (58)$$

with $a_i = \boldsymbol{a} - i$, $b_j = \boldsymbol{b} - j$ and $w = \boldsymbol{1}/\boldsymbol{1}_m$.

A RCE with a structure similar to equation (57) was given in reference [63]. A mechanical model composed of spring, dashpots and fractional elements is not known for this RCE.
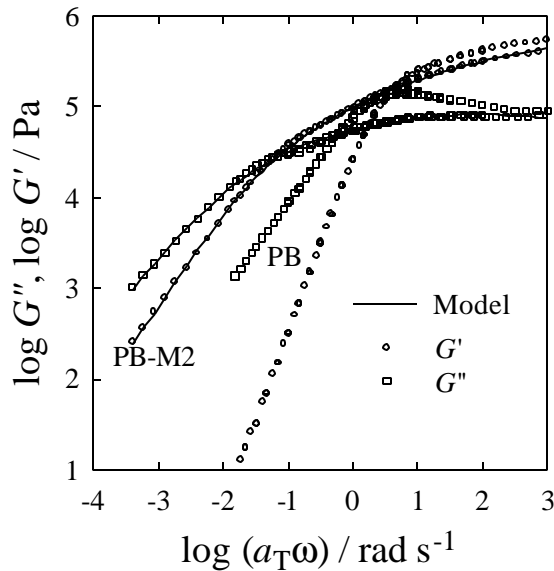

Figure 18. Storage $G'(a_T\boldsymbol{w})$ and loss modulus $G''(a_T\boldsymbol{w})$ for an unmodified (PB) and a sidechain modified polybutadiene (PB-M2), for details see reference [70]. The solid lines represent the fit according to equation (59) to the data.

6.2.2 Modification of $G^*(\omega)$ and of associated material functions

Another modification of polybutadienes leads to yet another behavior in the vicinity of the terminal region; instead of approaching the flow region after leaving the power law zone, a second power law is observed. We present in Figure 18 this behavior, which was the research object of reference [70]. Figure 18 shows the dynamic moduli of a polybutadiene which carries sidechains in a comb-like manner; the sidechains are mesogens, and are attached to the backbone via a flexible spacer. The polymer is in the isotropic state, but its branched molecular architecture and the interactions between the mesogens lead to a dynamic behavior quite different from that of linear chains, as can be seen from Figure 18.

Here the necessary modification to the material functions starts from the complex modulus $G^*(\omega)$. The two power law regions at the lowest frequencies are depicted by the FMM; multiplying $G^*_{\text{FMM}}(\boldsymbol{w})$ with an additional relaxation term leads to:

$$G^*(\boldsymbol{w}) = E \frac{(i\boldsymbol{w}\boldsymbol{l}_1)^a}{1 + (i\boldsymbol{w}\boldsymbol{l}_1)^{a-b}} \frac{1}{1 + (i\boldsymbol{w}\boldsymbol{l}_2)^g} \tag{59}$$

Now the other relaxation functions of the model can be calculated following the procedures outlined above. The relaxation modulus $G(t)$ and the creep compliance $J(t)$ turn out to be complex expressions, which can be found in reference [70]. Figure 18 shows that equation (58) reproduces successfully the data, as indicated by the fitting curve. We close by giving the RCE belonging to equation (58) [70]:

$$\boldsymbol{t}(t) + \boldsymbol{l}_1^a \frac{d^a \boldsymbol{t}(t)}{dt^a} + \boldsymbol{l}_2^g \frac{d^g \boldsymbol{t}(t)}{dt^g} + \boldsymbol{l}_1^a \boldsymbol{l}_2^g \frac{d^{a+g} \boldsymbol{t}(t)}{dt^{a+g}} = E\boldsymbol{l}_1^b \frac{d^b \boldsymbol{g}(t)}{dt^b} \ . \tag{60}$$

Hence the mechanical representation of this model is a combination of 4 FEs in series; these are of the form (x, E, λ), with $x = \beta$, $\beta - \alpha$, $\beta - \gamma$ and $\beta - \alpha - \gamma$.

7. CONCLUSIONS AND OUTLOOK

In this chapter we have shown how fractional calculus allows a physically sound generalization of classical models from the linear theory of viscoelasticity (see also the review by A. I. Leonov in this book). From a mathematical point of view, the operation of fractional integrodifferentiation is well defined and can be easily handled in Fourier or Laplace space. Viewed technically, integrodifferentiation allows, for instance, to interpolate smoothly between Hooke's and Newton's laws. Moreover, we have introduced the simplest form of a fractional rheological model, which we call fractional element (FE), and we have provided for it several mechanical analogs, namely arrangements made out of springs and dashpots. In these (infinite) networks the order of fractional integration or differentiation can be adjusted in several ways; say, by varying the material constants of the springs and dashpots involved, or by changing the structure of the arrangement.

Furthermore, we have shown how parallel or serial combinations of FEs lead to more complex models; in particular we have studied extensions of the Maxwell, the Kelvin-Voigt, the Zener and the Poynting-Thomson models. The relaxation patterns of these models can be used to fit the experimental results for large classes of materials. Particularly noticeable candidates are polymeric materials which display ramified structures (such as cross-linked polymers) or whose dynamics is characterized by cooperativity (i.e. glasses). Using fractional elements one can tailor viscoelastic models with given properties, while keeping the number of parameters involved relatively low.

The representation of generalized viscoelastic models by fractional analogues also allows a deeper insight into the physics behind fractional stress-strain relations. Nevertheless, we are still far from a reductionistic understanding of the fractional relaxation laws. Here, as well as in related areas, we expect much additional work in the coming years.

APPENDIX

Here we display some mathematical relations which are helpful in understanding the physical models of the Chapter. We start with the generalized Mittag-Leffler function which occurs, for instance, in the relaxation function of the fractional Maxwell model (equation(32)) or in the creep compliance of the fractional Kelvin-Voigt model (equation (35)). The generalized Mittag-Leffler function $E_{m,n}(z)$ is defined by [71]:

$$E_{\mu,\nu}(z) = \sum_{k=0}^{\infty} \frac{z^k}{\Gamma(\mu k + \nu)} \qquad \text{, with } \mu > 0 \text{ and } \nu > 0. \tag{61}$$

The special case $n = 1$ yields the usual Mittag-Leffler function $E_m(z)$. On the basis of this definition, the generalized Mittag-Leffler functions for some special cases, in which μ and ν equal 0.5, 1 or 2, follow readily:

$$E_{0.5,1}(z^{0.5}) = e^z \ \text{erfc}(-z^{0.5})$$

$$E_{0.5,2}(z^{0.5}) = \frac{1}{z}\left[e^z \ \text{erfc}(-z^{0.5}) - 1 - 2\left(\frac{z}{\boldsymbol{p}}\right)^{0.5} \right]$$

$$E_{1,1}(z^1) = e^z$$

$$E_{1,2}(z^1) = \frac{1}{z}[e^z - 1] \tag{62}$$

$$E_{2,1}(z^2) = \text{ch}(z)$$

$$E_{2,2}(z^2) = \frac{1}{z}\,\text{sh}(z) \ .$$

All generalized Mittag-Leffler functions increase monotonically for $z > 0$. To obtain monotonically decreasing functions one goes to the domain of negative z. In the parameter range $m, n \in (0,1]$ the following asymptotic expansions for $z \gg 1$ are of interest [26]:

$$E_{\mu,\mu}(-z) \propto \frac{\mu}{\Gamma(1-\mu)}\, z^{-2} \quad \text{for } \mu \neq 1 \tag{63}$$

$$E_{\mu,\nu}(-z) \propto \frac{1}{\Gamma(\nu-\mu)}\, z^{-1} \quad \text{for } \nu > \mu.$$

Consider now the relaxation function $G(t)$ of the FMM, equation (32). Here the generalized Mittag-Leffler function has the parameters $\mu = \alpha - \beta$ and $\nu = 1 - \beta$. From definition (61) and the asymptotic expansion (63) one obtains for the two power-law regimes:

$$G(t) \propto t^{-\beta} \qquad \text{for} \quad t \ll \lambda \tag{64}$$

$$G(t) \propto \begin{cases} t^{-\alpha} & (\alpha < 1) \\ t^{\beta-2} & (\alpha = 1) \end{cases} \quad \text{for} \quad t \gg \lambda \ .$$

In Figure 19 we show the relaxation function of the FMM, equation (32), for $\alpha = 1$ and $\beta = 0.5$. For the sake of comparison two other relaxation functions are added, which are different from the double power-law relaxation in the long time range.
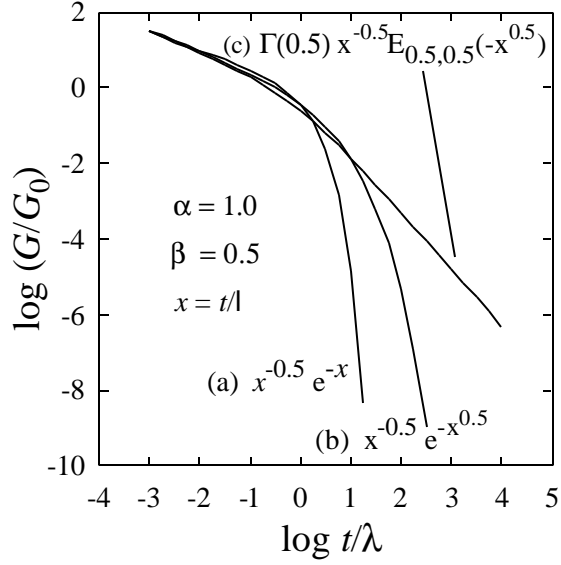
Figure 19. Dimensionless relaxation function $G(t)/G_0$ *vs* dimensionless time $t/\mathbf{1}$ for three models corresponding to different asymptotic behaviors: (a) exponential, (b) stretched exponential and (c) power-law.
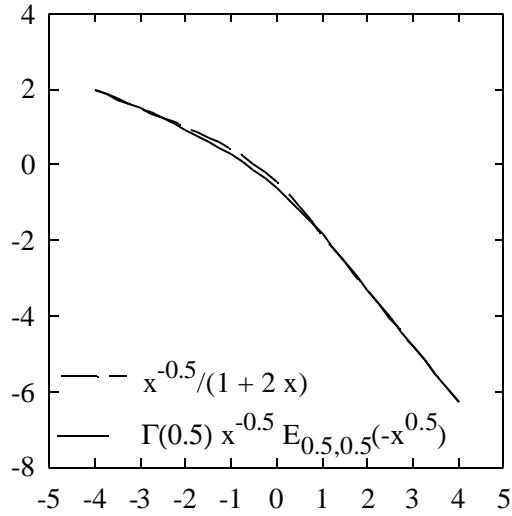

Figure 20. Comparison of a Mittag-Leffler function, lhs. of equation (65), with one of its Padé approximants, rhs. of equation (65).

The use of the generalized Mittag-Leffler function in numerical calculations is hampered due to the sometimes slow convergence of the series in equation (61). This can be taken care of by using a functional approximation; it turns out that Padé approximants allow to evaluate the generalized Mittag-Leffler functions almost exactly and without much effort. The procedure is described in [13]; in the lowest order approximation it yields exemplarily for $\alpha = 1$ and $\beta = 0.5$:

$$\boldsymbol{G}(0.5)\, E_{0.5,0.5}(-x^{0.5}) \approx \frac{1}{1+2\,x}\ . \tag{65}$$

The result is presented in Figure 20; note that deviations from the exact result are small and are restricted to the transition region between the power-law domains.

REFERENCES

1. R. Richert and A. Blumen (eds.), Disorder Effects on Relaxational Processes: Glasses, Polymers, Proteins, Springer, Berlin, 1994.
2. A. Blumen, in: Th. Dorfmüller and G. Williams (eds.), Molecular Dynamics and Relaxation Phenomena in Glasses, Springer, Berlin, 1987, p. 1.
3. J. Klafter, R. J. Rubin and M. F. Shlesinger (eds.), Transport and Relaxation in Random Materials, World Scientific, Singapore, 1986.
4. K. L. Ngai and G. B. Wright, Relaxation in Complex Systems, Naval Research Lab., Springfield, VA, 1984.
5. G. Williams and D. C. Watts, Trans. Faraday Soc., 66 (1970), 80; G. Williams, Adv. Polym. Sci., 33 (1979), 59.
6. F. Kohlrausch, Pogg Ann. Physik, 29 (1863), 337.
7. J. Friedrich and A. Blumen, Phys. Rev. B, 32 (1985), 1434.
8. A.V. Tobolsky and E. Catsiff, Journal of Polymer Science, 19 (1956), 111.
9. M. Mours and H.H. Winter, Chapter in this book.
10. Chr. Friedrich and H. Braun H., Colloid Polym. Sci., 272 (1994), 1536.
11. Chr. Friedrich, Rheol. Acta, 30 (1991), 151.
12. Chr. Friedrich, in: J. Casas-Vázquez and D. Jou (eds.), Rheological modelling: Thermodynamical and Statistical Approaches, Lecture Notes in Physics No. 381, Springer, Berlin, 1991, p. 321.
13. Chr. Friedrich and H. Braun, Rheol. Acta, 31 (1992), 309.
14. Chr. Friedrich and S. Hazanov, in: Advances in Structured and Heterogeneous Continua, Allerton Press Inc., New York, 1994, p. 173.
15. Chr. Friedrich and L. Heymann, J. Rheol., 32 (1988), 235.

16. Chr. Friedrich, L. Heymann and H.-R. Berger, Rheol. Acta, 28 (1989), 535.
17. Chr. Friedrich, J. Non-Newt. Fluid Mech., 46 (1993), 307.
18. Chr. Friedrich, Phil. Mag. Letters, 66 (1992), 287.
19. Chr. Friedrich, H. Braun and J. Weese, Polym. Eng. Sci., 35 (1995), 1661.
20. M. Caputo and F. Meinardi, Riv. Nuovo Cimento (Ser. 2), 1 (1971), 161.
21. F. Meinardi and E. Bonetti, Progress and Trends in Rheology II, Suppl. Rheol. Acta, 26 (1988), 64.
22. F. Meinardi, Fractional relaxation in anelastic solids, J. All. & Comp., 211/212 (1994), 534.
23. M. Abramowitz and I. A. Stegun (eds.), Handbook of Mathematical Functions, Dover, New York, 1972.
24. N.W. Tschoegl, The Phenomenological Theory of Linear Viscoelastic Behavior, Springer, Berlin, 1989.
25. I.M. Ward, Mechanical Properties of Solid Polymers, Wiley, Chichester, 1983.
26. K.B. Oldham and J. Spanier, The Fractional Calculus, Academic, New York, 1974.
27. K.S. Miller and B. Ross, An Introduction to the Fractional Calculus and Fractional Differential Equations, Wiley, New York, 1993.
28. A. Gemant, Physics, 7 (1936), 311.
29. A. Gemant, Phil. Mag. 25 (1938), 540.
30. P.G. Nutting, J. of the Franklin Institute, 191 (1921), 679.
31. P. G. Nutting, Proc. Amer. Soc. Test. Mater., 21 (1921), 1162.
32. P. Kobeko, E. Kuvshinskij and G. Gurevitch, Techn. Phys USSR, 4 (1937), 622.
33. A. P. Alexandrov and Yu. S. Lazurkin, J. Tech. Fiz., 9 (1939), 1250; 1261.
34. A. LeMehaute, L. Picard and L. Fruchter, Phil. Mag. B, 52 (1985), 1071.
35. G.W. Scott-Blair and F.M.V. Coppen, Amer. J. Psychol, 56 (1943), 234.
36. J.E. Caffyn and G.W. Scott-Blair, Nature, 155 (1945), 171.
37. G.W. Scott-Blair, B.C. Veinoglou and J.E. Caffyn, Proc. Roy. Soc. Ser. A, 189 (1947), 69.
38. G.W. Scott-Blair and J.E. Caffyn, Phil. Mag., 40 (1949), 80.
39. R.C.L. Bosworth, Nature, 157 (1946), 447.
40. G.L. Slonimsky, Journal of Polymer Science: Part C, 16 (1967), 1667.
41. W. Smit and H. de Vries, Rheol. Acta, 9 (1970), 525.
42. W.G. Glöckle and T.F. Nonnenmacher, Macromolecules, 24 (1991), 6426.
43. T.F. Nonnenmacher, in: J. Casas-Vázquez and D. Jou (eds.), Lecture Notes in Physics No. 381, Springer, Berlin, 1991, p. 309.
44. T.F. Nonnenmacher, W.G. Glöckle, Phil. Mag. Letters, 64 (1991), 89.
45. R.C. Koeller, J. Appl. Mech., 51 (1984), 299.

46. Y.N. Rabotnov, Elements of Hereditary Solid Mechanics, Mir Publishers, Moscow, 1980.
47. Chr. Friedrich and S. Hazanov, in: D.A. Siginer and Y.G. Yanovsky (eds.), Advances in Structured and Heterogeneous Continua, Allerton Press, New York, 1994.
48. R.L. Bagley, J. Rheol., 27 (1983), 201.
49. R.L. Bagley and P.J. Torvik, J. Rheol., 30 (1986), 133.
50. L. Rogers, J. Rheol., 27 (1983), 351.
51. W.E. VanArsdale, J. Rheol., 29 (1985), 851.
52. W.G. Glöckle, T.F. Nonnenmacher, Rheol. Acta, 33 (1994), 337.
53. R. Metzler, W. Schick, H.-G. Kilian and T.F. Nonnenmacher, J. Chem. Phys., 103 (1995), 7180.
54. H. Schiessel and A. Blumen, J. Phys. A, 26 (1993), 5057.
55. H. Schiessel, P. Alemany and A. Blumen, Progr. Colloid Polym. Sci., 96 (1994), 16.
56. H. Schiessel and A. Blumen, Macromolecules, 28 (1995), 4013.
57. H. Schiessel and A. Blumen, Fractals, 3 (1995), 483.
58. H. Schiessel, R. Metzler, A. Blumen and T.F. Nonnenmacher, J. Phys. A, 28 (1995), 6567.
59. J.-C. Bauwens, Colloid Polym. Sci. 270 (1992), 537.
60. N. Heymans and J.-C. Bauwens, Rheol. Acta, 33 (1994), 210.
61. N. Heymans, Rheol. Acta, 35 (1996), 508.
62. M. Giona, S. Cerbelli and H.E. Roman, Physica A, 191 (1992), 449.
63. J. Stastna, L. Zanzotto and K. Ho, Rheol. Acta 33 (1994), 344.
64. M. Odenwald, H.-F. Eicke and Chr. Friedrich, Colloid Polym. Sci., 274 (1996), 568; M. Odenwald, Diploma-Thesis, Freiburg 1993.
65. Chr. Friedrich and H. Dehno, in: Progress and Trends in Rheology IV, Steinkopffverlag, Darmstadt, 1994, p. 45.
66. L.I. Palade, V. Verney and P. Attane, Rheol. Acta, 35 (1996), 265.
67. S. Hellinckx, Colloid Polym. Sci., 275 (1997), 116.
68. S. Havlin and A. Bunde, in: A. Bunde and S. Havlin (eds.), Fractals and Disordered Systems, Springer, Berlin, 1991, p. 97.
69. M. Mours and H.H. Winter, Macromolecules, 29 (1996), 7221.
70. Chr. Friedrich, Acta Polymerica, 46 (1995), 385.
71. A. Erdélyi (ed.), Bateman Manuscript Project, Higher Transcendental Functions, Vol. III, Mc.Graw-Hill, New York, 1955.